J Neurophysiol 104: 1020–1033, 2010.
First published June 16, 2010; doi:10.1152/jn.01129.2009.

The *h* Current Is a Candidate Mechanism for Regulating the Sliding Modification Threshold in a BCM-Like Synaptic Learning Rule

Rishikesh Narayanan and Daniel Johnston
Center for Learning and Memory, The University of Texas, Austin, Texas

Submitted 21 December 2009; accepted in final form 16 June 2010

Narayanan R, Johnston D. The *h* current is a candidate mechanism for regulating the sliding modification threshold in a BCM-like synaptic learning rule. *J Neurophysiol* 104: 1020–1033, 2010. First published June 16, 2010; doi:10.1152/jn.01129.2009. Hebbian synaptic plasticity acts as a positive feedback mechanism and can destabilize a neuronal network unless concomitant homeostatic processes that counterbalance this instability are activated. Within a Bienenstock-Cooper-Munro (BCM)-like plasticity framework, such compensation is achieved through a modification threshold that slides in an activity-dependent fashion. Although the BCM-like plasticity framework has been a useful formulation to understand synaptic plasticity and metaplasticity, a mechanism for the activity-dependent regulation of this modification threshold has remained an open question. In this simulation study based on CA1 pyramidal cells, we use a modification of the calcium-dependent hypothesis proposed elsewhere and show that a change in the hyperpolarization-activated, nonspecific-cation *h* current is capable of shifting the modification threshold. Based on the direction of such a shift in relation to changes in the *h* current, and supported by previous experimental results, we argue that the *h* current fits the requirements for an activity-dependent regulator of this modification threshold. Additionally, using the same framework, we show that multiple voltage- and ligand-gated ion channels present in a neuronal compartment can regulate the modification threshold through complex interactions among themselves. Our results underscore the heavy mutual interdependence of synaptic and intrinsic properties/plasticity in regulating learning and homeostasis in single neurons and their networks under both physiological and pathological brain states.

INTRODUCTION

Activity-dependent modifications to the rules of synaptic plasticity, defined as metaplasticity, are now an established form of plasticity in the nervous system (Abraham 2008; Abraham and Bear 1996; Abraham and Tate 1997; Bear 2003). Theoretical origins of this form of plasticity can be traced back to the Bienenstock-Cooper-Munro (BCM) rule (Bienenstock et al. 1982). The BCM rule was originally proposed for the development of orientation selective cells in the visual cortex, but later has been linked to metaplasticity mechanisms associated with long-term potentiation (LTP) and depression (LTD) (Abraham 2008; Bear 2003). According to the BCM rule, a neuron possesses a synaptic modification threshold (denoted as θ_m), which dictates whether its activity at any given instant leads to potentiation or depression of its synapses. Whereas the neuron's active synapses grow stronger when postsynaptic activity exceeds θ_m, it gets weaker when activity falls below θ_m (but remains above an LTD threshold).

More importantly, to incorporate competition and provide stability, the BCM rule sets θ_m as a sliding threshold, a threshold that is dynamic and is dependent on average postsynaptic activity. This sliding threshold acts as a homeostatic mechanism that retains the modifiable synapses within a useful dynamic range (Abraham 2008; Abraham and Bear 1996; Abraham and Tate 1997; Abraham et al. 2001). Specifically, it acts against the Hebbian positive feedback mechanism, a process, which, if uncontrolled, leads to synapses either growing infinitely, or being set to zero by repetitive LTP or LTD, respectively. The sliding threshold neutralizes this by acting as a negative feedback mechanism: θ_m increases if the postsynaptic activity is high, thus making LTP more difficult, and LTD easier, to induce. Hence, if postsynaptic activity is high, although the synapses may undergo LTP as a result of correlated activity, their ability to undergo additional LTP is comparatively reduced. An inverse process occurs when postsynaptic activity is reduced: θ_m decreases, thus making LTD more difficult, and LTP easier, to induce. Thus in the presence of such activity-dependent modification of the plasticity rule, synapses avoid unstable configurations of infinite growth or infinite reduction.

There have been various proposals on the mechanisms underlying this sliding threshold (Abraham 2008; Abraham and Bear 1996; Abraham and Tate 1997; Bear 1995). Prominent among them are changes in *N*-methyl-D-aspartate receptor (NMDAR) subunit composition (Philpot et al. 2001), in NMDAR signaling (Philpot et al. 2003), in calcium buffering (Gold and Bear 1994), and in CaMKII levels (Bear 2003; Mayford et al. 1995). Here, we show that the hyperpolarization-activated, nonspecific-cation *h* current (I_h) is capable of shifting θ_m by regulating intracellular calcium influx during plasticity induction. Then, based on recent experimental results from our laboratory and others (Brager and Johnston 2007; Campanac et al. 2008; Fan et al. 2005; Narayanan and Johnston 2007), we propose the *h* current as a candidate mechanism for controlling the sliding modification threshold in a BCM-like plasticity rule. Finally, we show that the sliding modification threshold is not just a function of the *h* current, but can be modified by multiple voltage- and ligand-gated ion channels. In addition to providing a broad framework toward understanding the role of intrinsic properties in modulating synaptic metaplasticity, our study also underscores the heavy mutual interdependence of synaptic and intrinsic properties/plasticity in regulating learning and homeostasis in single neurons and their networks.

METHODS

To simplify computational cost and avoid the dependence of plasticity mechanisms on the location of synapses (Froemke et al. 2005; Saudargiene et al. 2005), we used a single compartment model

Address for reprint requests and other correspondence: D. Johnston, Ctr. for Learning and Memory, The Univ. of Texas at Austin, 1, University Station Stop, C7000, Austin, TX 78712-0805 (E-mail: djohnston@mail.clm.utexas.edu).

to study the impact of changes in the *h* current on plasticity mechanisms. The NEURON simulation environment (Carnevale and Hines 2006) was used to perform all the simulations with an integration time constant of 25 μs.

A single compartment of length 50 μm and diameter 1 μm (Fig. 1*A*) was used to approximate a dendrite 200 μm away from the soma. The passive parameters were set as those for a dendrite (Gasparini et al. 2004): $R_m = 28$ kΩ.cm^2 and $C_m = 1.5$ μF/cm^2. Na, KDR, KA, and *h* channels were introduced, with kinetics the same as those used in Gasparini et al. 2004. Default values of parameters were set as follows: reversal potentials (in mV), $E_h = -30$, $E_K = -90$, $E_{Na} = 55$; maximum conductance densities (in mS/cm^2), $\bar{g}_{Na} = 30$, $\bar{g}_{KDR} = 5$, $\bar{g}_{KA} = 44$, $\bar{g}_h = 42$. The default values of the maximum conductance densities were obtained from (Gasparini et al. 2004) for a dendrite located at 200 μm away from the soma. The kinetics for the *h* and Na^+ channels were shifted according to the specifications of Gasparini et al. (2004) for a dendrite located at 200 μm away from the soma. All simulations were performed at −65 mV.

Synapse model

A synapse was modeled as a co-localized combination of NMDA and AMPA receptor currents, with parameters as given below. A spike generator was used to feed inputs to this synapse at the requisite frequency. The default value of NMDA:AMPA ratio was set at 1.5.

The current through the NMDA receptor, as a function of voltage and time, is dependent on three ions: sodium, potassium, and calcium. Consequently, as per the Goldman-Hodgkin-Katz convention, we write

$$I_{NMDA}(v,t) = I^{Na}_{NMDA}(v,t) + I^{K}_{NMDA}(v,t) + I^{Ca}_{NMDA}(v,t) \quad (1)$$

where

$$I^{Na}_{NMDA}(v,t) = \bar{P}_{NMDA} P_{Na}\, s(t) MgB(v) \frac{vF^2}{RT} \left\{ \frac{[Na]_i - [Na]_o \exp\left(-\frac{vF}{RT}\right)}{1 - \exp\left(-\frac{vF}{RT}\right)} \right\} \quad (2)$$

$$I^{K}_{NMDA}(v,t) = \bar{P}_{NMDA} P_{K}\, s(t) MgB(v) \frac{vF^2}{RT} \left\{ \frac{[K]_i - [K]_o \exp\left(-\frac{vF}{RT}\right)}{1 - \exp\left(-\frac{vF}{RT}\right)} \right\} \quad (3)$$

$$I^{Ca}_{NMDA}(v,t) = \bar{P}_{NMDA} P_{Ca}\, s(t) MgB(v) \frac{4vF^2}{RT} \left\{ \frac{[Ca]_i - [Ca]_o \exp\left(-\frac{2vF}{RT}\right)}{1 - \exp\left(-\frac{2vF}{RT}\right)} \right\} \quad (4)$$

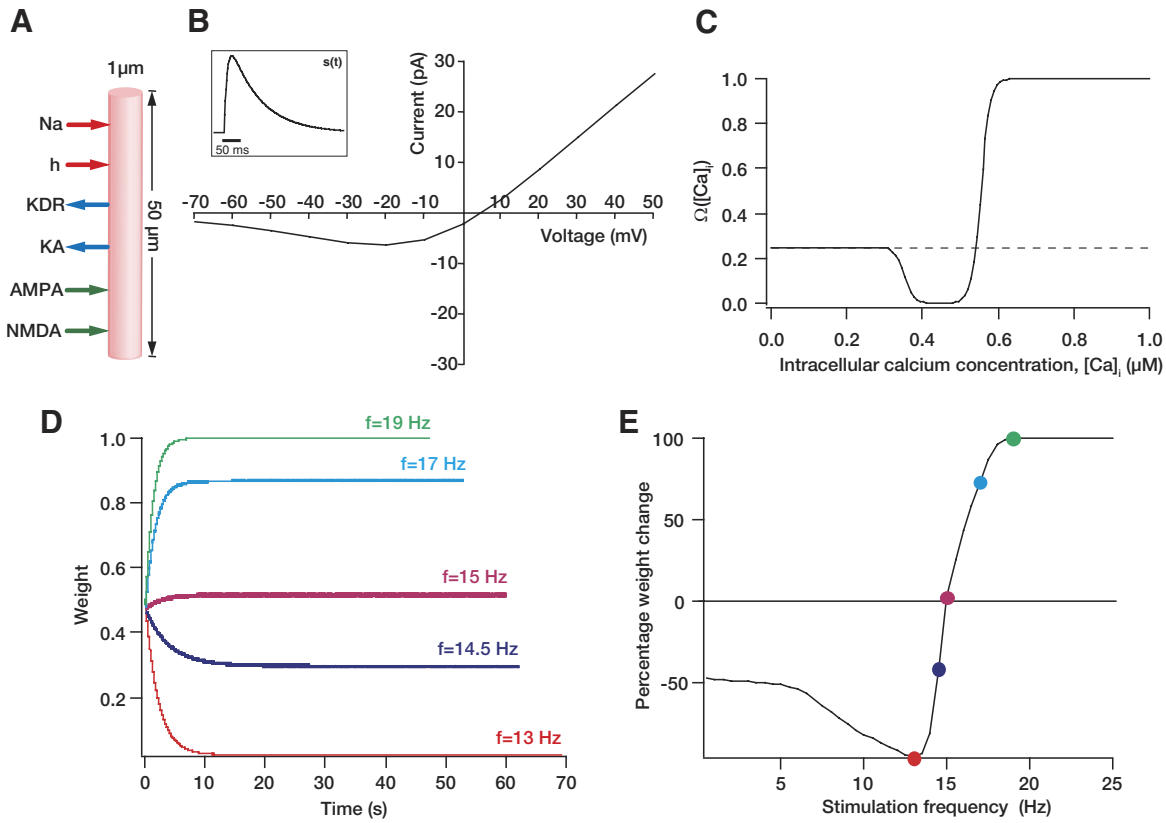

FIG. 1. Illustration of the basics of our model. *A*: schematic of the single compartment model used in this study. The various ligand- and voltage-gated channels used in the model are depicted as arrows. *B*: properties of *N*-methyl-D-aspartate receptor (NMDAR) current used in the model. The current through the receptor as a function of membrane voltage shows the magnesium dependent voltage block at hyperpolarized voltages. *Inset*: time course of a typical NMDAR excitatory postsynaptic potential (EPSP). *C*: functional form of the plasticity-regulating Ω-function plotted for various concentrations of intracellular calcium. *D*: evolution of weight *w*, when the model was stimulated with 900 pulses of multiple frequencies, plotted as a function of time. It may be noted that the evolution approximates an exponential. The color codes for various frequencies translate to *E* as well. Because 900 pulses of a low-frequency stimulus ended later than 900 pulses of a high-frequency stimulus, the endpoints are variable. It may be noted that at the end of the stimulus protocol, the weight parameter increased (potentiation) for frequencies that are approximately >15 Hz while decreasing (depression) for frequencies lesser than that value. *E*: plot obtained by tracking percentage change in weight *w* after 900 pulses of stimulus at various frequencies. The colored dots represent the values obtained from *D* for corresponding frequencies.

where $\bar{P}_{NMDA}$ is the maximum permeability of the NMDA receptor. $P_{Ca} = 10.6$, $P_{Na} = 1$, and $P_K = 1$, owing to the permeability of the NMDA receptor to different ions being $P_{Ca}:P_{Na}:P_K = 10.6:1:1$ (Canavier 1999; Mayer and Westbrook 1987). Default values of concentrations were (in mM) $[Na]_i = 18$, $[Na]_o = 140$, $[K]_i = 140$, $[K]_o = 5$, $[Ca]_i = 100 \times 10^{-6}$, $[Ca]_o = 2$. The concentrations for sodium set its equilibrium potential at +55 mV and that for potassium at −90 mV. Evolution of intracellular calcium with NMDA-dependent calcium current σ^{Ca}_{NMDA} and its buffering was modeled as in (Poirazi et al. 2003)

$$\frac{d[Ca]_i}{dt} = -\frac{10,000\, I^{Ca}_{NMDA}}{3.6 \cdot dpt \cdot F} + \frac{[Ca]_\infty - [Ca]_i}{\tau_{Ca}} \quad (5)$$

where F is Faraday's constant, $\tau_{Ca} = 30$ ms is the calcium decay constant, $dpt = 0.1$ μm is the depth of the shell, and $[Ca]_\infty = 10^{-4}$ mM is the steady-state value of $[Ca]_i$. $MgB(v)$ governs the magnesium dependence of the NMDA current (Fig. 1*B*), given as (Jahr and Stevens 1990)

$$MgB(v) = \left\{1 + \frac{[Mg]_o \exp(-0.062v)}{3.57}\right\}^{-1} \quad (6)$$

with the default value of $[Mg]_o$ set at 2 mM. $s(t)$ governs the kinetics of the NMDA current and is given as (Fig. 1*B*)

$$s(t) = a\left[\exp\left(-\frac{t}{\tau_d}\right) - \exp\left(-\frac{t}{\tau_r}\right)\right] \quad (7)$$

where a is a normalization constant, making sure that $0 \leq s(t) \leq 1$, τ_d is the decay time constant, τ_r is rise time with $\tau_r = 5$ ms, and $\tau_d = 50$ ms. Figure 1*B* provides the voltage dependence and time course of the NMDA current obtained with this model.

In general, in pyramidal cells, current through the AMPA receptor, as a function of voltage and time, is dependent on two ions: sodium and potassium. Consequently, we modeled the current through the AMPA receptor as a sum of currents carried by these two ions

$$I_{AMPA}(v, t) = I^{Na}_{AMPA}(v, t) + I^{K}_{AMPA}(v, t) \quad (8)$$

where

$$I^{Na}_{AMPA}(v, t) = \bar{P}_{AMPA}\, w P_{Na}\, s(t) \frac{vF^2}{RT}\left\{\frac{[Na]_i - [Na]_o \exp\left(-\frac{vF}{RT}\right)}{1 - \exp\left(-\frac{vF}{RT}\right)}\right\} \quad (9)$$

$$I^{K}_{AMPA}(v, t) = \bar{P}_{AMPA}\, w P_{K}\, s(t) \frac{vF^2}{RT}\left\{\frac{[K]_i - [K]_o \exp\left(-\frac{vF}{RT}\right)}{1 - \exp\left(-\frac{vF}{RT}\right)}\right\} \quad (10)$$

where $\bar{P}_{AMPA}$ is the maximum permeability of the AMPA receptor, whose default value was set at 10 nm/s. P_{Na} was taken to be equal to P_K, given experimental observations (Dingledine et al. 1999). w is the weight parameter that undergoes activity-dependent update. $s(t)$ was the same as that for the NMDA receptor, but with $\tau_r = 2$ ms and $\tau_d = 10$ ms.

Weight update mechanism

Synaptic weight parameter w (see *Eqs. 9* and *10*) was updated as a function of intracellular calcium, following the calcium control hypothesis (Shouval et al. 2002). Specifically

$$\frac{dw}{dt} = \eta([Ca]_i)[\Omega([Ca]_i) - w] \quad (11)$$

where, $\eta([Ca]_i)$ is the calcium-dependent learning rate, inversely related to the learning time constant $\tau([Ca]_i)$

$$\eta([Ca]_i) = \frac{1}{\tau([Ca]_i)} \quad (12)$$

$$\tau([Ca]_i) = P_1 + \frac{P_2}{P_3 + [Ca]_i^{P_4}} \quad (13)$$

with $P_1 = 1$ s, $P_2 = 0.1$ s, $P_3 = P_2 \times 10^{-4}$, and $P_4 = 3$. This takes into account that when $[Ca] \approx 0$, $\tau([Ca]_i) \approx 3$ h (Shouval et al. 2002). $\Omega([Ca]_i)$ has the following form (Fig. 1*C*)

$$\Omega([Ca]_i) = 0.25 + \frac{1}{1 + \exp\{-\beta_2([Ca]_i - \alpha_2)\}} - 0.25\frac{1}{1 + \exp\{-\beta_1([Ca]_i - \alpha_1)\}} \quad (14)$$

with $\alpha_1 = 0.35$, $\alpha_2 = 0.55$, $\beta_1 = 80$, and $\beta_2 = 80$. In all of the above weight update equations, for compatibility, $[Ca]_i$ is set as $[Ca]_i - 100$ nM. Unless otherwise stated, the default initial value of w, w_{init}, was set at 0.5.

RESULTS

Synaptic plasticity is bidirectional in nature, and the associated mechanisms and signaling pathways are complex (Derkach et al. 2007; Flavell and Greenberg 2008; Johnston et al. 2003; Kennedy et al. 2005; Kerchner and Nicoll 2008; Lisman 1989, 2009; Lisman and Raghavachari 2006; Malenka and Bear 2004; Massey and Bashir 2007; Newpher and Ehlers 2008; Sacktor 2008; Shepherd and Huganir 2007). Computational models that are built toward understanding various aspects of synaptic plasticity thus use simplifying assumptions or enlist abstractions so that the problem becomes tractable, while still providing insights into brain function (Abbott and Nelson 2000; Ajay and Bhalla 2006; Bienenstock et al. 1982; Kalantzis and Shouval 2009; Lisman and Raghavachari 2006; Shouval et al. 2002; Song et al. 2000; Willshaw and Dayan 1990). Our study extends the model presented in (Shouval et al. 2002), but significantly differs in terms of the use of conductance-based models for voltage-gated channels and in terms of the models for the glutamate receptors (see METHODS). Consequent to this extension, the assumptions that are inherent to the model presented in Shouval et al. (2002) also extend to our model. Specifically, our model inherits the calcium control hypothesis that states that different calcium levels trigger different forms of synaptic plasticity (Lisman 1989) and also considers NMDA receptors as the sole source of calcium (Shouval et al. 2002). While the latter assumption is still permissive to generalization within the modeling framework, the former is more restrictive because it is known that multiple parameters including intracellular locations of signaling molecules, rates associated with multiple reaction-diffusion systems, kinetics of calcium entry, and the expression of various kinases and phosphatases contribute to the direction and strength of synaptic plasticity (Ajay and Bhalla 2006; Derkach et al. 2007; Flavell and Greenberg 2008; Johnston et al. 2003; Kennedy et al. 2005; Kerchner

and Nicoll 2008; Lisman 2009; Lisman and Raghavachari 2006; Liu et al. 2004; Malenka and Bear 2004; Massey and Bashir 2007; Newpher and Ehlers 2008; Sacktor 2008; Shepherd and Huganir 2007). The amount of NMDAR-dependent calcium influx plays a crucial role in synaptic plasticity (Bear 2003; Bear et al. 1987; Lisman 1989, 2001; Lisman and Raghavachari 2006; Zucker 1999), and the calcium control hypothesis has proven as an useful abstraction to understand multiple plasticity-related phenomena (Kalantzis and Shouval 2009; Shah et al. 2006; Shouval et al. 2002; Yeung et al. 2004; Yu et al. 2008). Thus in this study, we used the calcium control hypothesis, together with its underlying assumptions, to establish a broad framework to understand the role of voltage-gated ion channels in modulating synaptic plasticity.

Generating the synaptic plasticity profile using the model

We induce plasticity in the model synapse by presenting 900 stimuli (through a spike generator associated with the synapse) at a given frequency. Using this framework, the direction and strength of plasticity were analyzed by presenting stimuli made of 900 pulses at various frequencies (0.5–25 Hz) to the model (Dudek and Bear 1992; Johnston et al. 2003; Shouval et al. 2002). Such stimulation of co-localized NMDAR–AMPAR synapse would lead to changes in intracellular calcium concentration depending on the stimulus frequency and various other parameters associated with the model. This, is turn, would affect the calcium-dependent weight update process as in *Eq. 11*. The evolution of weights as given by *Eq. 11* is monitored (Fig. 1*D*), and the final weight at the end of the induction protocol is noted down for each frequency. The percentage difference between this final weight and the initial weight (0.5) is plotted against the frequency of the stimulus pulses to obtain the synaptic plasticity profile as a function of stimulus frequency (Shouval et al. 2002). Figure 1*E* provides an example of such a plasticity profile generated with our model.

The h current induces a saturating rightward shift to the plasticity profile

As a first step of our analysis, we increased the maximum value of the *h* conductance, $\bar{g}_h$, progressively and generated the plasticity profile for each of its values. We observed a rightward shift in the plasticity profile with an increase in $\bar{g}_h$ (Fig. 2*A*). We used the sliding modification threshold (θ_m) as a measure to quantify the relationship between this shift and $\bar{g}_h$. A plot of θ_m versus $\bar{g}_h$ (Fig. 2*B*) fits an exponential function ($\tau = 0.71$ $\mu S/cm^2$), indicating that the rightward shift (increase in θ_m) induced by an increase in $\bar{g}_h$ saturates beyond a certain point. Together these indicate that an increase in *h* current can produce a saturating rightward shift to the BCM-like synaptic learning rule.

Reasoning that any change in the plasticity profile should, under this framework, be dependent on the intracellular concentration of calcium, we looked at the total levels (area under the curve) of intracellular calcium influx through the induction protocol (900 pulses of a given frequency of stimulation) for various values of $\bar{g}_h$. As expected, increases in $\bar{g}_h$ reduced the levels of intracellular calcium across the range of frequencies of stimulation, with the effects being more pronounced in the higher frequencies of stimulation (Fig. 2*C*). This is to be expected because increases in $\bar{g}_h$ reduce temporal summation (Magee 1998, 1999) and the amount of calcium entering through the NMDA receptor. To quantify further this de-

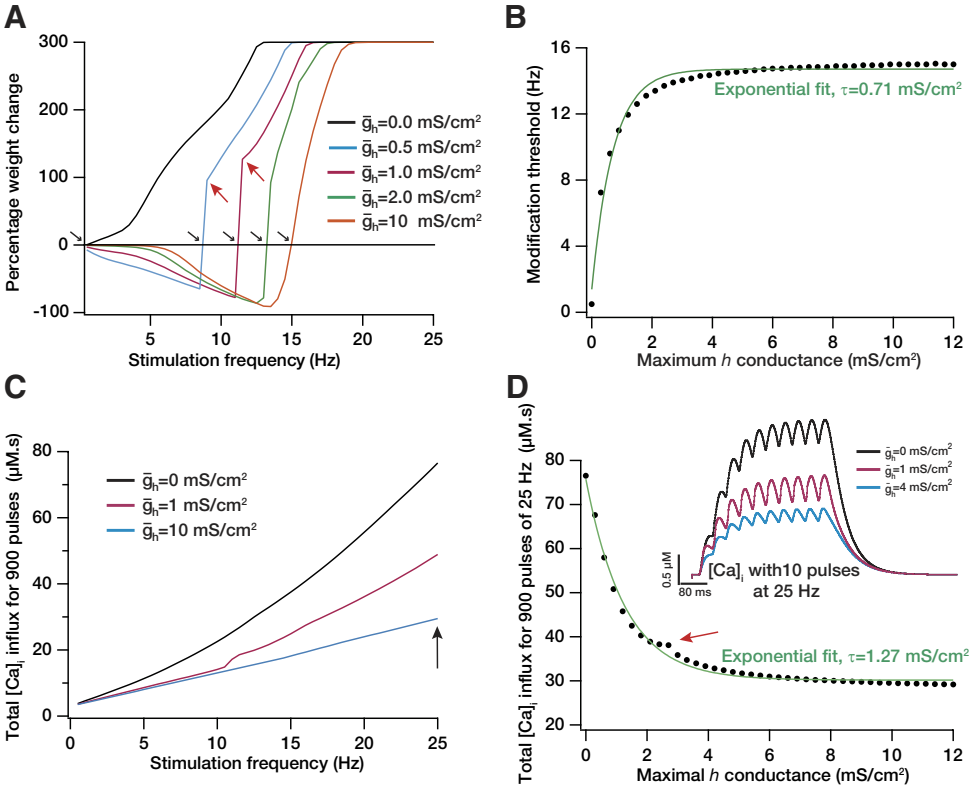

FIG. 2. Increase in the *h* current produced a saturating rightward shift to the Bienenstock-Cooper-Munro (BCM)-like synaptic plasticity profile through reduction in intracellular calcium influx. *A*: percentage weight change induced by 900 stimulus pulses at various frequencies plotted as a function of the stimulus frequency for different values of maximal *h*-channel conductance, $\bar{g}_h$. A progressive rightward shift in the curve may be noted with increases in $\bar{g}_h$. $w_{init} = 0.25$ for these simulations (see Supplementary Fig. S2). *B*: quantifying the modification threshold, θ_m (indicated by black arrows in *A*), as a function of $\bar{g}_h$ shows a saturating rightward shift in the BCM-like plasticity profile with increase in $\bar{g}_h$. $w_{init} = 0.25$ for these simulations (see Supplementary Fig. S2). *C*: total calcium influx (area under the curve) obtained after 900 pulses of synaptic stimulation at a given frequency plotted as a function of the frequency of stimulation. The plots for various values of $\bar{g}_h$ indicate the reduction of calcium influx with increase in $\bar{g}_h$. *D*: total calcium influx at the end of 900 pulses of 25 Hz synaptic stimulation plotted as a function of $\bar{g}_h$. *Inset*: an illustration with typical traces of intracellular calcium obtained with 10 pulses of 25 Hz synaptic stimulation with 3 different values of $\bar{g}_h$. It may be noted that a higher value of $\bar{g}_h$ leads to a reduction in intracellular calcium levels. All red arrows indicate the point at which compartment switched from generating a spike to generating a subthreshold EPSP.

pendence of intracellular calcium on $\bar{g}_h$, we plotted the average intracellular calcium at the end of 900 pulses of the 25 Hz stimuli as a function of $\bar{g}_h$ and found an exponential reduction in the levels of calcium influx with increasing $\bar{g}_h$ (Fig. 2*D*). Thus the shift in modification threshold induced by an increase in $\bar{g}_h$ is mediated through a reduction in excitability and a consequent reduction in the amount of calcium influx through NMDA receptors.

Modulation in *h* channel properties need not be only associated with the maximal conductance (the number of channels). Modulation could also occur through changes in the half-maximal activation voltage and/or through changes in activation time constant, for instance, through changes in subunit composition and/or channel phosphorylation state (Biel et al. 2009; Pape 1996; Robinson and Siegelbaum 2003). Thus it is essential to ask if the modification threshold is dependent only on the maximal *h* channel conductance, or is it also sensitive to other parameters associated with the *h* channel. To answer this question, we systematically varied various parameters associated with the *h* channel and assessed their role in altering the modification threshold. We found that, whereas the modification threshold was sensitive to the half-maximal activation voltage ($V_{1/2}$) of the *h* channel (Fig. 3, *A* and *B*), it was not as sensitive to the (de)activation time constant of the *h* channel for the protocols that we used for inducing plasticity. The dependence of the modification threshold on the $V_{1/2}$ of the *h* channel can be explained by the amount of *h* current at −65 mV (the voltage at which simulations are performed) with various values of $V_{1/2}$. Given the activation properties of *h* channels (Magee 1999), a lower value of $V_{1/2}$ (say, −150 mV; see Fig. 3*B*) would mean almost zero *h* current at −65 mV, whereas a higher value (say, 0 mV) would mean almost maximal conductance of *h* channels at −65 mV. Consequently, given Fig. 2 and our observations there about excitability and calcium, it would be expected that the modification threshold would be lower at hyperpolarized values of $V_{1/2}$ and increases with depolarization in $V_{1/2}$ (Fig. 3*B*). Thus depolarization in $V_{1/2}$ would shift the plasticity profile toward the right, making the induction of LTP more difficult. However, the (de)activation time constant was not as effective in shifting the plasticity profile (Fig. 3, *C* and *D*). This is to be expected because given the protocol we used for inducing plasticity (900 pulses of various frequencies), and given the frequency range where the modification threshold is (around 5–15 Hz), there is no significant temporal summation on the postsynaptic side, thus making the role of the *h* channel time constant very minimal.

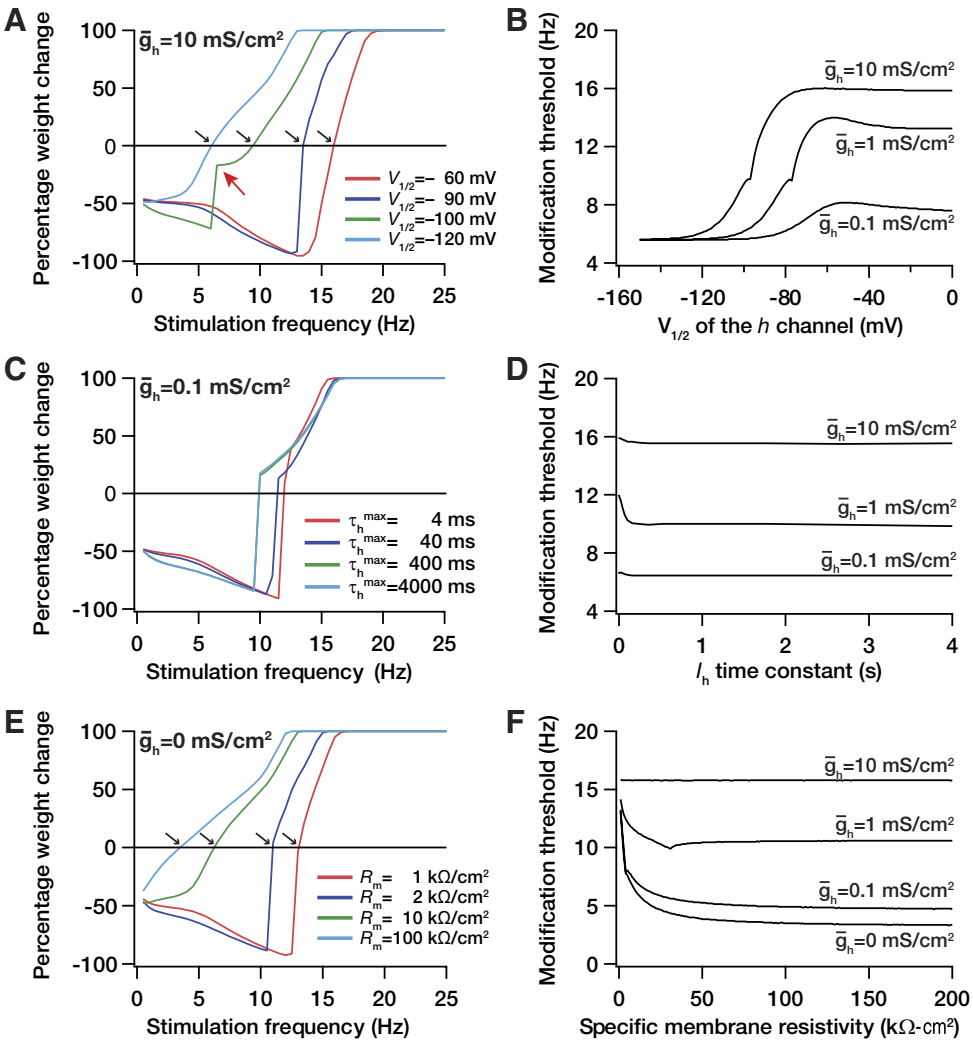

FIG. 3. Dependence of modification threshold on parameters associated with the model. Percentage weight change induced by 900 stimulus pulses at various frequencies plotted as a function of the stimulus frequency for different values of the half-maximal activation voltage $V_{1/2}$ of the *h* conductance (*A*), *h* channel (de)activation time constant (*C*), and specific membrane resistivity (*E*). The values of maximal *h*-channel conductance $\bar{g}_h$ for each of these cases are provided on the *top* of the individual panels. The modification threshold as a function of the half-maximal activation voltage $V_{1/2}$ of the *h* conductance (*B*), *h* channel (de)activation time constant (*D*), and specific membrane resistivity (*F*), each plotted for various values of maximal *h*-channel conductance $\bar{g}_h$.

We have shown that the shift in modification threshold induced by an increase in $\bar{g}_h$ is mediated through a reduction in excitability and consequent reduction in the amount of calcium influx through NMDA receptors (Fig. 1). Using our model, we next asked if the *h* channel was unique in its ability to shift the modification threshold through such a mechanism. To do this, we changed the leak conductance in the model to modulate excitability and asked whether this would change the modification threshold. Quite expectedly, an increase in leak conductance was able to shift the modification threshold toward the right (Fig. 3, *E* and *F*), owing to its ability to reduce excitability. Together, the ability of these conductances to bidirectionally modulate the modification threshold suggest that, in general, changes that lead to increased excitability would shift the modification threshold to the left, whereas those that reduce excitability shift the modification threshold to the right (also see dependence on *A*-type potassium channels, below).

If excitability were reduced by an increase in leak conductance, would the model still be amenable to changes in the *h* conductance? To test this, we reduced the leak conductance to 80–320 $\Omega.cm^2$, bringing the input resistance of the compartment to 50–200 MΩ, respectively. When we did this, we were still able to increase the modification threshold through increases in *h* conductance, thus confirming the results with higher leak conductances as well (Supplementary Fig. S1).[1]

Finally, we also tested if our results were dependent on the initial value of the weight parameter *w*, w_{init}. We found that, although the exact values of modification threshold and the amount of potentiation were different (consistent with Shouval et al. 2002) with different values of w_{init}, the shift in modification threshold as a function of changes in maximal *h* conductance was in the same direction and had the same dependencies across various values of w_{init} (Supplementary Fig. S2).

Dependence of modification threshold on multiple voltage-gated ion channels

Because changes in the *A*-type potassium current can also accompany various forms of synaptic plasticity (Frick et al. 2004; Kim et al. 2007; Losonczy et al. 2008), we assessed the role of the *A*-current on the plasticity profile. As a potassium conductance whose increase would reduce excitability, the expectation was that there would be a leftward shift in the plasticity profile with increases in the *A*-current. Obtaining plasticity profiles for various values of maximal *A*-type potassium channel conductance, $\bar{g}_{KA}$, however, showed a complex dependence of θ_m on $\bar{g}_{KA}$, with multiple ion channels contributing to the exact nature of such dependence (Fig. 4). Specifically, for lower values of $\bar{g}_h$, increases in $\bar{g}_{KA}$ initially led to a reduction in θ_m, implying a leftward shift in the plasticity profile (until the threshold transition point, indicated by arrows in Fig. 4*A*); however, with further increase in $\bar{g}_{KA}$, after a threshold, θ_m increased (Fig. 4*A*; e.g., curve corresponding to $\bar{g}_h = 0.75$ mS/cm^2). For higher values of $\bar{g}_h$, the effect of $\bar{g}_{KA}$ on the plasticity profile progressively reduced to finally become negligible (Fig. 4*A*; e.g., curve corresponding to $\bar{g}_h = 3$ mS/cm^2).

While the increase in θ_m with increases in $\bar{g}_{KA}$ during the latter part of the graph (beyond the transition point; indicated by red arrows) could be explained by the fact that $\bar{g}_{KA}$ is a potassium conductance, we were puzzled by the reduction in θ_m with increases in $\bar{g}_{KA}$ during the initial portion of the curve. We thus analyzed the reason behind this switch in the direction by closely examining the anatomy of a single ($\bar{g}_h = 0.75$ mS/cm^2) biphasic curve. Consider the case before the transition point (Fig. 4*B*, *left*), and take the case of the lower value of $\bar{g}_{KA}$ (=3 μS/cm^2). The plots of the model response to three pulses at 33 Hz shows a spike in response to each of the three stimuli. The activation of the delayed rectifier potassium channel should be noted, along with the calcium response through the NMDA receptors (Fig. 4*B*). When the value of $\bar{g}_{KA}$ is increased to 20 μS/cm^2, but still staying to the left of the transition point, this relatively higher value of $\bar{g}_{KA}$ produced a reduction in spike amplitude (Hoffman et al. 1997; Migliore et al. 1999). This reduction in spike amplitude led to a lower activation of the delayed rectifier, as observed from the conductance plot in Fig. 4*B*. Thus because of the smaller potassium influx (through the delayer rectifier potassium channel), the calcium response was not "shunted," and thus there was an increase in the amount of calcium influx, eventually leading to a reduction in the modification threshold. An increase in $\bar{g}_{KA}$ in this regimen increased calcium influx through reduction of spike amplitude with the consequent reduction of the delayed rectifier potassium conductance. These results also suggest a novel role for the *A*-current in that it could regulate spike-induced reset of excitatory postsynaptic potentials (EPSPs) (Hausser et al. 2001) through its ability to regulate spike amplitude. Such regulation of spike-induced reset can act as a variable reset of synaptic integration in hippocampal neurons. Given the location dependence of *A*-type K^+ current in hippocampal neurons (Hoffman et al. 1997), such reset of synaptic integration would also be location-dependent, making different regions of the neuron contribute differently to synaptic integration during dendritic spikes or backpropagating action potentials (Hausser et al. 2001).

Now, consider the regimen beyond the transition point (Fig. 4*B*, *right*). During this regimen, there were no spikes, and the EPSPs summated to let calcium influx into the cell. Because there were no spikes in this case, there was no activation of the delayed rectifier potassium conductance, thus making only the subthreshold conductances play a role in determining the modification threshold. Now, with an increase in $\bar{g}_{KA}$ (from 80 to 150 μS/cm^2), there was a reduction in temporal summation leading to reduction in calcium influx (Fig. 4*B*). Thus during this regimen, an increase in $\bar{g}_{KA}$ decreased calcium influx through reduction of temporal summation of EPSPs. Thus our simulation results indicate that the switch occurs when the compartment ceases to elicit a spike. In other words, increases in $\bar{g}_{KA}$ led to a reduction in θ_m if spikes were elicited and an increase in θ_m if spikes were not elicited.

The progressive leftward shift observed in the threshold for the switch (indicated by arrows in Fig. 4*A* and plotted in Fig. 4*C*) with increased $\bar{g}_h$ can also be explained as follows: with increases in $\bar{g}_h$,the excitability of the compartment was reduced. This reduction suppressed spiking in the compartment with even a smaller value of $\bar{g}_{KA}$, thus leading to the observed decrease in this threshold as a function of $\bar{g}_h$ (Fig. 4*C*). Finally, when $\bar{g}_h$ was high enough, there was no value of $\bar{g}_h$ where spikes could be elicited, thus leading to the absence of any such switch in the direction of change (Fig. 4*A*; $\bar{g}_h = 3$ mS/cm^2).

[1] The online version of this article contains supplemental data.

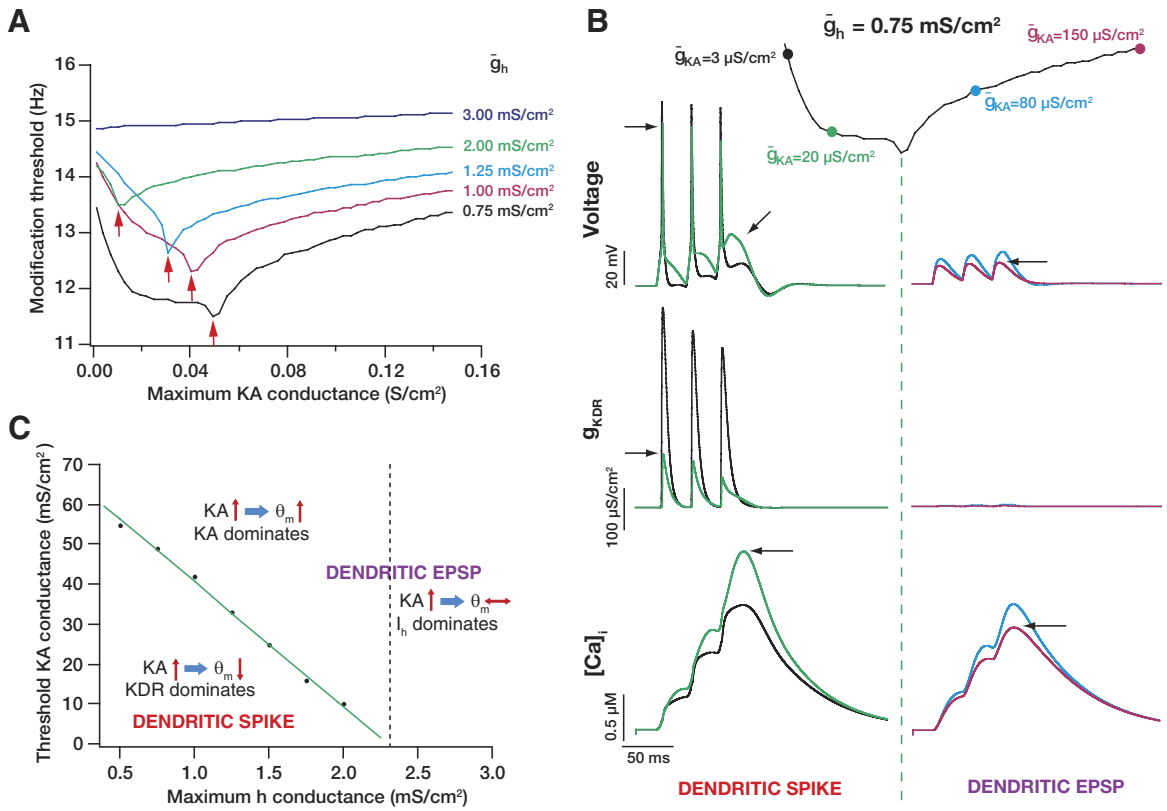

FIG. 4. Dependence of modification threshold on multiple voltage-gated ion channels. *A*: the modification threshold as a function of maximal *A*-type potassium channel conductance, $\bar{g}_{KA}$, plotted for various values of maximal *h* channel conductance $\bar{g}_h$. Red arrows indicate the point at which compartment switched from generating a spike to generating a subthreshold EPSP (see *B*). *B*: anatomy of a single curve in *A* (corresponding to $\bar{g}_h = 0.75$ mS/cm^2, given on the *top*), showing the basis for the biphasic nature of the plots in *A*. In the regimen of the plot (area left to the green dotted line) where there was a decrease (leftward shift of the BCM-like plasticity profile) in the modification threshold with an increase in $\bar{g}_{KA}$, there were local spikes (*top*) in response to 3 pulses at 33 Hz, thus activating the delayed rectifier potassium channels (*middle*). In the regimen of the plot (area right to the green dotted line) where there was an increase (rightward shift of the BCM-like plasticity profile) in the modification threshold with an increase in $\bar{g}_{KA}$, there were no local spikes (*top*), thus there was no activation of the delayed rectifier potassium (KDR) channels (*middle*). It may be noted that the calcium influx increased with increases in $\bar{g}_h$ in the region where the delayed rectifier channels were activated, whereas it decreased with increases in $\bar{g}_{KA}$ in the region where the KDR channels were not activated (*bottom*). This may be observed from the black arrows that indicate the traces corresponding to the increased value of $\bar{g}_h$ in each of the 2 cases. *C*: plot showing relative dominance of the 3 channels under consideration in determining the modification threshold. The plot shows the value of minimum modification threshold (indicated by red arrows in *A*) as a function of $\bar{g}_{KA}$. Toward the left of this threshold, there were dendritic spikes, and the consequent activation of the delayed rectifier channels made it the prominent channel in determining the calcium influx and thus the modification threshold. Toward the right of it, the balance between $\bar{g}_{KA}$ and $\bar{g}_h$ determine the modification threshold.

Together, it may be noted that the modification threshold was dependent on the multiple conductances depending on their relative conductance values. These dependencies are summarized in Fig. 4*C*, where the threshold transition point is plotted as a function of $\bar{g}_h$. To the left of the linear plot, there were dendritic spikes, thus making the delayed rectifier conductance dominate (Fig. 4*B*, *left*). In this regimen, an increase in the *A*-type conductance led to a reduction of the modification threshold. Toward the *right* of this linear plot, there were no spikes. Here, until a certain transition value of $\bar{g}_h$ (represented by dotted lines), the *A*-type potassium current dominated where increases in the A-type current led to an increase in the modification threshold (Fig. 4*A*). Beyond this transition value of $\bar{g}_h$, changes in $\bar{g}_{KA}$ had very little effect on the modification threshold, thus making $\bar{g}_h$ the dominant force.

Our analysis of the *A*-current thus far has considered only changes in $\bar{g}_{KA}$. However, there are reports of changes in the *A*-current effectuated through a shift in its inactivation curve (Frick et al. 2004). Specifically, that study reported a localized shift in the inactivation curve of the *A*-type potassium channel (from −63.5 to −69.2 mV, on an average) accompanying LTP. We asked if a shift in the inactivation curve of the *A*-type potassium channel could alter the modification threshold and induce metaplasticity in hippocampal synapses. To do this, we calculated the modification threshold for various values of the $V_{1/2}$ of the inactivation curve of the *A*-type potassium channel and plotted this as a function $V_{1/2}$ (Fig. 5). We found that a shift in the inactivation curve of the *A*-type potassium channels behaved in a fashion similar to the increase in $\bar{g}_{KA}$ (Fig. 5). Specifically, we observed a biphasic curve where the modification threshold decreased until a certain transition value of the inactivation $V_{1/2}$ and increased beyond that value. This transition point was a function of the value of $\bar{g}_h$, with a progressive decrease in the transition value of the inactivation $V_{1/2}$ with increase in $\bar{g}_h$. Finally, beyond a certain value of $\bar{g}_h$, the inactivation $V_{1/2}$ had very little effect on the modification threshold. Thus the modification threshold as a function of the inactivation $V_{1/2}$ behaved in a similar fashion to its dependence on $\bar{g}_{KA}$. Together, these results suggest the modification threshold is regulated through complex interactions between multiple voltage-gated ion channels. The exact nature of these dependencies and interactions are contingent on individual channel

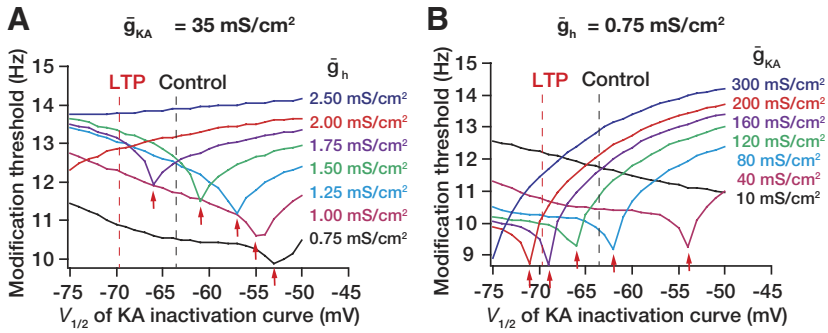

FIG. 5. Interplay between the *A*-type potassium current and the *h* current in determination of modification threshold. *A*: modification threshold, θ_m, as a function of the inactivation $V_{1/2}$ of the *A*-type potassium conductance, for various values of maximum *h* conductance (at a given $\bar{g}_{KA}$ = 35 mS/cm^2). *B*: θ_m as a function of the inactivation $V_{1/2}$ of the *A*-type potassium conductance, for various values of maximum *A*-type potassium conductance (at a given $\bar{g}_h$ = 0.75 mS/cm^2). Red arrows in *A* and *B* indicate the points at which there was a switch (from progressive decrease to increase) in θ_m as a function of the inactivation $V_{1/2}$ of the *A*-type potassium conductance. The vertical lines in *A* and *B* named control and LTP refer to the values of the inactivation $V_{1/2}$ of the *A*-type potassium conductance reported by (Frick et al. 2004) before and after LTP. All red arrows indicate the point at which compartment switched between generating a spike to generating a subthreshold EPSP.

properties and conductance values and their relationships to those of the other ion channels in the same compartment.

Increase in glutamate receptor permeability shifts the plasticity profile to the left

A large body of evidence suggests an increase in AMPA receptor density follows induction of LTP (Andrasfalvy and Magee 2004; Derkach et al. 2007; Kerchner and Nicoll 2008; Malenka and Bear 2004; Shepherd and Huganir 2007). Furthermore, the density of AMPA receptors are known to increase with distance of the dendritic location from the soma, and this has been suggested as a mechanism for the normalization of location dependence of EPSPs in Schaffer collateral synapses (Andrasfalvy and Magee 2001; Smith et al. 2003). To assess any potential influence of AMPA receptor density on the plasticity profile, we generated the profile for various values of the AMPA receptor permeability. It is expected that the depolarization offered by higher AMPA receptor could relieve the magnesium block in NMDA receptor, thus leading to an increased calcium influx through the NMDA receptors. Conforming to this expectation (Shouval et al. 2002), we observed that increase in AMPA receptor permeability led to a leftward shift in the plasticity profile (Fig. 6*A*). To quantify further this relationship, we plotted θ_m as a function of AMPA receptor permeability. We observed that there was an approximately linear reduction in the sliding threshold of the plasticity profile as a function of AMPA receptor permeability (Fig. 6*B*). Next, given that NMDARs are important for the induction of plasticity, and given that there could be changes in NMDARs as a result of certain activity pattern, we asked whether changes in NMDAR density could alter the plasticity profile. Again, conforming to results by Shouval et al. (2002), our results suggested that increases in NMDAR density would shift the plasticity profile to the left (Fig. 6*C*).

Together our results suggest that the plasticity profile of a synapse located in a dendritic segment is dependent on the properties of voltage-gated channels present in that dendritic segment and the ligand-gated channels at a particular synapse.

DISCUSSION

A primary conclusion of this study is that a change in the hyperpolarization-activated *h* current is capable of shifting the plasticity profile within a BCM-like learning framework. Specifically, our results suggest that an increase in the *h* current would shift the plasticity profile toward the right, increasing the sliding modification threshold, whereas a decrease would accomplish the opposite (Fig. 2). With this background, we analyzed recent results from our laboratory on plasticity in the

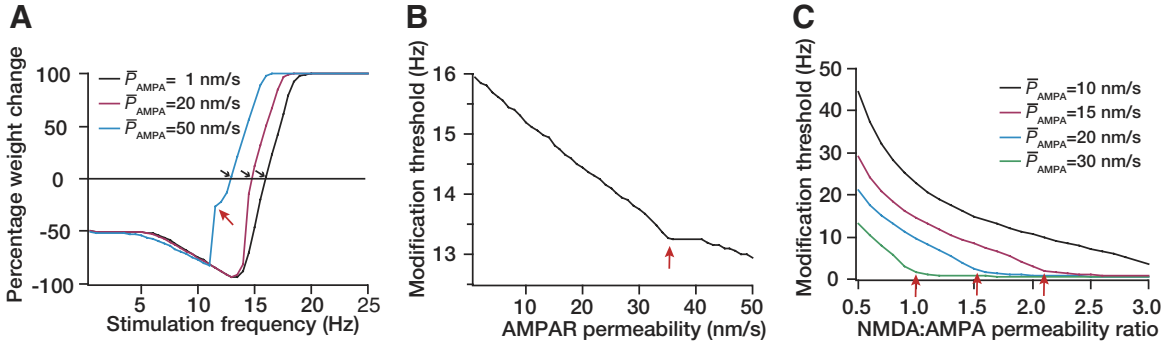

FIG. 6. Increase in glutamate receptor permeability shifted the BCM-like plasticity profile to the left. *A*: percentage weight change induced by 900 pulses of stimuli at various frequencies plotted as a function of the stimulus frequency for various values of AMPA receptor (AMPAR) permeability. A progressive leftward shift in the BCM-like plasticity profile may be noted with increase in AMPAR permeability. *B*: plotting the modification threshold, θ_m, as a function of AMPAR permeability indicates an approximately linear relationship between the 2, until the compartment starts eliciting spikes (point denoted by an arrow). *C*: plotting θ_m as a function of NMDAR permeability suggests a similar relationship. The plot is shown for various values of AMPAR permeability. All red arrows indicate the point at which compartment switched from generating an EPSP to generating a spike.

h current that accompanies synaptic plasticity in hippocampal pyramidal neurons. It has been shown that LTP is accompanied by an increase in the *h* current (Fan et al. 2005), and that a decrease in the *h* current accompanies LTD (Brager and Johnston 2007). We argue that these results in conjunction with results from this study make the *h* current a candidate for mediating the sliding modification threshold within a BCM-like framework (Fig. 7). To elaborate, consider first the LTP case. Within a BCM framework, an increase in postsynaptic activity (consequent to LTP of certain synapses) should shift the plasticity profile to the right, thus reducing the possibility of further potentiation and retaining the dynamic range of synapses within a useful range (Bienenstock et al. 1982). Experimental results have demonstrated that LTP is accompanied by an increase in the *h* current (Fan et al. 2005; Narayanan and Johnston 2007), and our results show that increases in the *h* current shift the plasticity profile to the right. Together, this fits the BCM-like framework, where LTP would be accompanied by an increase in the sliding modification threshold. The LTD case would just be the antipode for this with experiments showing a reduction in the *h* current with LTD (Brager and Johnston 2007) and that this reduction would lead to a leftward shift in the plasticity profile (Fig. 2). Hence, the *h* current can mediate a rightward shift in the plasticity profile accompanying LTP-inducing stimuli and a leftward shift accompanying LTD-inducing stimuli, exactly in the manner required by a BCM-like plasticity framework to maintain modifiable synapses of the network within a useful dynamic range.

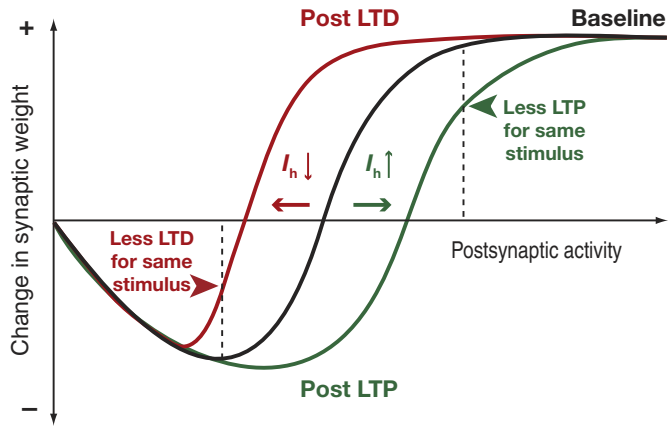

FIG. 7. Summary diagram showing the role of the *h* current in bidirectional regulation of the sliding modification threshold and the consequent retention of the dynamic range of synapses. In the absence of a homeostatic mechanism, synaptic strength would increase to saturation with repeated potentiation and would reduce to 0 in the case of repeated depression. However, when a concurrent increase in the *h* current accompanies long-term potentiation (LTP) (Fan et al. 2005), this shifts the plasticity profile to the right (green arrow, and plasticity profile in green), thus reducing the ability of the same stimulus to induce further LTP (green arrowhead), and reducing the possibility of synaptic saturation. Long-term depression (LTD), on the other hand, is accompanied by a reduction in the *h* current (Brager and Johnston 2007), which would lead to a leftward shift to the plasticity profile (red arrow, and plasticity profile in red), thus reducing the ability of the same stimulus to induce further LTD (red arrowhead) and reducing the possibility of synaptic retraction/death. Within a BCM-like framework, LTP would be accompanied by a rightward shift in the plasticity profile, whereas LTD would be accompanied by a leftward shift. Here, an increase in the *h* current shifts the plasticity profile toward the right, whereas a decrease in the *h* current shifts it to the left. Previous experimental results have shown an increase in the *h* current accompanying LTP and a decrease in the same accompanying LTD. Taken together, these results imply that LTP is accompanied by a rightward shift in the plasticity profile, whereas LTD is accompanied by a leftward shift. This matches with the requirements for the sliding modification threshold within a BCM-like synaptic learning framework, thus establishing the *h* current as a candidate mediator of the sliding modification threshold.

An important requirement of the sliding modification threshold in a BCM-like plasticity framework is that the changes need to be global in nature, affecting all synapses even if the associated plasticity is local (Bienenstock et al. 1982; Turrigiano and Nelson 2000). Matching this, the increase in the *h* current accompanying LTP has been experimentally shown to be spatially widespread even if the associated LTP was pathway specific (Narayanan and Johnston 2007). Specifically, using recordings from the apical dendritic shaft (up to ~300 μm), we directly assessed measurements sensitive to the *h* current and showed that the changes in *h* channels accompanying LTP are spatially widespread. Furthermore, we also showed that synaptic potentiation in one pathway reduces temporal summation in an unpotentiated pathway onto the same neuron, thus directly showing the heterosynaptic nature of the effects of changes in *h* channels. With LTD, direct dendritic measurements of the *h* current-dependent measurements have not been performed. However, experiments involving two-pathway LTD showing heterosynaptic changes in a nondepressed pathway (Brager and Johnston 2007) and modeling results suggesting that only somatic changes in the *h* current are insufficient to induce large changes in excitability (Narayanan and Johnston 2007) support the conclusion that *h* current changes accompanying LTD are also spatially widespread. Thus because changes in *h* current that accompany synaptic plasticity span huge dendritic distances and act heterosynaptically (Brager and Johnston 2007; Narayanan and Johnston 2007), and because the *h* current can bidirectionally shift the plasticity profile in a manner required by a BCM-like framework (Figs. 2 and 3), we suggest that the *h* current is a candidate mechanism for regulating the sliding modification threshold within a BCM-like synaptic learning framework (Fig. 7).

Although frameworks based on the BCM model (Bienenstock et al. 1982) have been very useful in understanding synaptic plasticity rules and metaplasticity (Gold and Bear 1994; Kalantzis and Shouval 2009; Shah et al. 2006; Shouval et al. 2002; Yeung et al. 2004; Yu et al. 2008), it should be noted that the experimental evidence for the presence and regulation of a sliding modification threshold (within the realms of the synaptic plasticity framework) is inferential and indirect (Abraham 2008; Abraham and Bear 1996; Abraham and Tate 1997; Abraham et al. 2001; Bear 2003; Cooper et al. 2004; Holland and Wagner 1998; Kirkwood et al. 1996; Philpot et al. 2001, 2003; Wang and Wagner 1999). Furthermore, although the calcium-dependent plasticity framework used in this study and others (Kalantzis and Shouval 2009; Shah et al. 2006; Shouval et al. 2002; Yeung et al. 2004; Yu et al. 2008) derives inspiration from the BCM framework, the BCM framework and the Hebbian synaptic plasticity framework in Schaffer collateral synapses are not completely analogous to each other (Cooper et al. 2004). There are numerous differences between them including those on what they model, on how they effectuate changes in the sliding modification threshold, and on how they link the sliding modification threshold to plasticity and metaplasticity (see Cooper et al. 2004 for a detailed analysis on the differences). We used the term "BCM-like" throughout the manuscript to take into con-

sideration the fact that our synaptic plasticity framework, whereas it draws inspiration from the BCM framework, is not the same as the BCM framework. In what follows, we present some implications of our results, along with some experimentally testable predictions that follow from our study.

The h current as the mediator of the sliding modification threshold: Implications

As inferred from our results, the regulation of the plasticity profile by the *h* current is not achieved by directly controlling the synaptic currents or by signaling pathways associated with plasticity as proposed earlier (Abraham and Tate 1997; Bear 1995), but through its ability to modulate dendritic excitability (Magee 1998; Narayanan and Johnston 2007). In other words, the modulation of the *h* current alters the local response properties around the synapse, thus leading to the regulation of the plasticity profile through modulation of the amount of calcium entering into the cell during a plasticity-inducing stimulus. This offers a prediction, which could be tested through the measurement of calcium influx into a cell during a plasticity-inducing stimulus with and without *h*-channel blockers.

The *h* current as a candidate for controlling the modification threshold offers multiple advantages over other possible mechanisms in terms of homeostasis. For instance, it has been earlier shown that increases in the *h* current can lead to a reduction in the postsynaptic firing (Poolos et al. 2002). Thus increases/decreases in the *h* current could also act to neutralize the increase/decrease in synaptic weights with LTP/LTD and bring about firing rate homeostasis in the postsynaptic cell (Turrigiano and Nelson 2000). Furthermore, with its known ability to control temporal integration (Magee 1998, 1999), changes in *h* current could also effectively modulate temporal integration of a response across temporally spaced episodes of synaptic activity (Abraham and Bear 1996). Finally, the *h* current also acts as a phenomenological inductance (Narayanan and Johnston 2008) and renders band-pass characteristics to the local and transfer impedances in multiple neurons (Hu et al. 2002, 2009; Hutcheon and Yarom 2000; Narayanan and Johnston 2007; Ulrich 2002). Changes in *h* current, accompanying synaptic plasticity would thus alter the frequency-dependent response properties of the neuron, which has been postulated to endow a neuron with the ability to match its response properties to stimulus statistics (Narayanan and Johnston 2007) and providing independent control to a single neuron over temporal coding of incoming information (Narayanan and Johnston 2008). Thus the *h* current acting as a controller of the sliding threshold not only keeps the synapses in the dynamic functional range (through regulation of the plasticity profile), but also could help in maintaining firing rate homeostasis, alter frequency-dependent response properties, change calcium-response properties, and modulate temporal integration depending on the network activity profile (Biel et al. 2009).

Plasticity in voltage-gated ion channels and metaplasticity

Our results showed that the sliding modification threshold is also a function of the properties of multiple voltage- and ligand-gated ion channels. This shows the complex interactions between synaptic and intrinsic properties in determining information processing within single neurons and their networks. For instance, synaptic plasticity is accompanied by changes in voltage-gated ion channels (Brager and Johnston 2007; Campanac et al. 2008; Fan et al. 2005; Frick et al. 2004; Losonczy et al. 2008; Narayanan and Johnston 2007; Sjostrom et al. 2008), and these changes in voltage-gated ion channels can alter the rules behind the induction of synaptic plasticity, thus closing a feedback loop of interactions between synaptic and intrinsic properties. Such feedback loops have important implications toward maintaining homeostasis and retaining the dynamic range of synapses and neuronal firing rates (Abraham 2008; Turrigiano 1999; Turrigiano and Nelson 2000; Yeung et al. 2004).

The role of metaplasticity triggered by changes in voltage-gated ion channel properties should be taken into account while interpreting experiments involving the use of multiple protocols for inducing synaptic plasticity (Abraham 2008; Abraham and Bear 1996; Abraham and Tate 1997; Chung et al. 2009). To elaborate, experiments that study the saturation of synaptic plasticity (Bliss and Lomo 1973; Huang and Malenka 1993; McNaughton et al. 1978; Schulz et al. 1994), depotentiation (Barrionuevo et al. 1980; Fujii et al. 1991), and synaptic capture (Barco et al. 2002; Sajikumar et al. 2005) require the use of multiple protocols that induce synaptic plasticity. Consider the case where the first such induction is accompanied by changes—in either a spatially localized (Frick et al. 2004; Losonczy et al. 2008; Wang et al. 2003) or widespread (Narayanan and Johnston 2007) manner—in a voltage-gated ion channel that is capable of modifying the plasticity profile of synapses. Now, synapses in these regions would have undergone metaplasticity and thus would adhere to a different plasticity rule that they would have in the absence of such changes in voltage-gated ion channel properties. Thus in interpretation of experiments that involve multiple induction protocols, it is important to assess for changes in voltage-gated ion channels as well, and ask if there was a metaplastic shift associated with any of such induction protocols. This is extremely important because the same protocols that lead to synaptic plasticity also lead to changes in multiple ion channels and follow similar signaling pathways (Campanac et al. 2008; Chung et al. 2009; Fan et al. 2005; Frick et al. 2004; Kim et al. 2007; Losonczy et al. 2008; Lujan et al. 2009; Rosenkranz et al. 2009; Wang et al. 2003), thus establishing an extremely tight, strongly interlinked feedback system involving both synaptic and intrinsic properties in the regulation of neuronal plasticity and homeostasis (Turrigiano and Nelson 2000; Zhang and Linden 2003). Finally, spine structure, another variable regulated by synaptic plasticity (Alvarez and Sabatini 2007), has recently been put forward as a putative mediator of metaplasticity (Kalantzis and Shouval 2009). Thus given that structural, intrinsic, and synaptic properties could change with synaptic plasticity (Alvarez and Sabatini 2007; Brager and Johnston 2007; Campanac et al. 2008; Fan et al. 2005; Frick et al. 2004; Lisman 2009; Malenka and Bear 2004; Shepherd and Huganir 2007; Sjostrom et al. 2008) and could also play a role in inducing metaplasticity (Figs. 2–6) (Kalantzis and Shouval 2009; Shouval et al. 2002), extreme care should be taken in interpreting experiments involving multiple plasticity protocols that follow one another.

Apart from changes in voltage-gated ion channels accompanying synaptic plasticity, changes in the voltage-gated ion chan-

nels have also been reported through development (Moody and Bosma 2005) and during pathological conditions such as epilepsy and ischemia (Beck and Yaari 2008; Bernard et al. 2007). Given that multiple ion channels can modulate the sliding modification threshold, are there changes in the rules of synaptic plasticity that accompany any of these conditions (Crepel et al. 2003; Errington et al. 1995; Kemp et al. 2000; Leite et al. 2005; Reid and Stewart 1997; Turrigiano and Nelson 2004)? How are these changes related to voltage-gated ion channels modulation? The answers to these questions are important, especially given the important roles that the interactions between synaptic balance and intrinsic properties play in maintaining or impeding homeostasis during development or pathological conditions (Beck and Yaari 2008; Scharfman 2007; Turrigiano and Nelson 2004). Future experiments could thus focus on understanding the roles of voltage-gated ion channels and intrinsic properties in inducing metaplasticity during development and pathological conditions.

Somato-dendritic gradients in voltage-gated ion channels and metaplasticity

Whereas plasticity in ion channels associated with physiological or pathological conditions represents one layer of complexity, another layer of complexity arises from the gradients in properties and densities of various voltage-gated ion channels along the somato-dendritic axis of a single hippocampal pyramidal neuron. Various ion channels, including the *h* channel (Lorincz et al. 2002; Magee 1998), the *A*-type potassium channel (Hoffman et al. 1997), the *M*-type potassium channel (Hu et al. 2007), the G protein–coupled inward rectifying potassium (GIRK) channels (Chen and Johnston 2005), and the AMPA receptor (Andrasfalvy and Magee 2001; Smith et al. 2003), have gradients in their densities changing as the function of distance from the soma (Johnston and Narayanan 2008; Migliore and Shepherd 2002). With more than one ion channel capable of controlling the modification threshold (Figs. 2–6), how does this differential distribution of ion channels affect the modification threshold as a function of distance from the soma? There are at least two possible answers to this question.

The first possibility is that there are various computational subunits along the dendritic tree (Losonczy et al. 2008; Poirazi et al. 2003; Polsky et al. 2004; Williams 2004), with each of them endowed with their own independent modification threshold depending on the local distribution and properties of various ion channels. This would be a departure from the classical BCM rule, where there is only one modification rule governing the entire neuron. Such location dependence of the modification threshold would raise the possibility that a stimulus that evokes LTP in a dendritic region near the soma could elicit LTD in a dendritic region away from the soma. Such a possibility would be consistent with various experimental reports: *1*) the presence of various computational subunits within a neuron (Losonczy et al. 2008; Poirazi et al. 2003; Polsky et al. 2004; Williams 2004); *2*) the distance dependence of various forms of synaptic plasticity, owing, in some cases, to changes in channel distribution (Froemke et al. 2005; Sjostrom and Hausser 2006; Sjostrom et al. 2008); *3*) the localized nature of some forms of activity-dependent plasticity in voltage-gated ion channels (Frick et al. 2004; Losonczy et al. 2008; Wang et al. 2003), which implies that the effects of such plasticity on modification threshold also will remain localized; and *4*) localized nature of most forms of synaptic plasticity (Bliss and Collingridge 1993; Malenka and Bear 2004; Watt et al. 2004) would imply localized changes in modification threshold owing to the ability of AMPAR and NMDAR to change the modification threshold (Fig. 6).

A second possibility is that, despite variations of densities of these channels (both voltage- and ligand-gated) capable of controlling the modification threshold, there could be normalization of plasticity rules across the neuron or at least across the stratum radiatum, where the Schaffer collaterals form synapses. Such a possibility could arise because the gradient in one of the components could actively neutralize the gradient in another, thus enforcing the same plasticity rule across the region of concern. For instance, the gradient in AMPA receptor density has been proposed to neutralize location dependence of synapses (Andrasfalvy and Magee 2001; Smith et al. 2003), whereas the gradient in *h* channels has been proposed to normalize synaptic integration (Magee 1999). However, it may be noted from our results that increases in AMPAR and *h* current induce opposite changes to the modification threshold. One possibility is that they neutralize each other by proportional increases across the dendritic regions so that plasticity in the concerned region is uniform. Such a scheme may be implemented because of the confluence of multiple ion channel gradients within the dendrite, which are mutually coupled to enforce it. Future experiments could focus on analyzing the role of various ion channels in inducing metaplasticity and answering the question about which of the two aforementioned possibilities is implemented by a hippocampal neuron.

The primary focus of this study was on the *h* channels and their role in regulating the sliding modification threshold (Figs. 2–3 and 7), although the cross-dependencies on the leak channels (Figs. 3 and S1), the *A*-type potassium current (Figs. 4 and 5), and glutamate receptors (Fig. 6) were also analyzed. Dependencies on a large number of other channels have not been analyzed in this study, including calcium channels and other potassium channels including the GIRK and calcium-activated potassium channels, despite their known roles in mediating or regulating synaptic plasticity (Johnston et al. 1992; Lujan et al. 2009). Furthermore, we only considered one form of plasticity induction with 900 pulses of various frequencies (Dudek and Bear 1992; Johnston et al. 2003; Shouval et al. 2002) throughout our study, without considering other forms of plasticity like spike timing– or pairing-dependent forms of synaptic plasticity. Thus the basic quantitative framework developed in this study for understanding the role of voltage-gated ion channels in modulating synaptic plasticity forms a foundation for the analysis of the role of various ion channels in different forms of inducing plasticity. Finally, it should also be noted that this framework is designed specifically for plasticity in the Schaffer collateral synapses in hippocampal CA1 pyramidal neurons and would not necessarily extend to other synapses or to other brain regions. For instance, in the parallel fibers synapses of the cerebellar Purkinje neurons, the plasticity rule is inverse of a BCM-like synaptic learning rule, where lower levels of calcium influx induce LTP, with higher levels inducing LTD (Jorntell and Hansel 2006). Thus while our basic framework could be extended toward quantitatively understanding plasticity in other synapses, extreme caution should be exercised in extending the results to other synapses because the constitutive components and the dynamical rules can be different across different neurons.

To summarize, we proposed the *h* current as a candidate mediator for the sliding modification threshold within a BCM-like plasticity framework, based on computational simulations, with experimental support on bidirectional activity-dependent changes in the *h* current accompanying bidirectional synaptic plasticity (Brager and Johnston 2007; Campanac et al. 2008; Fan et al. 2005; Narayanan and Johnston 2007). Our results and analyses also establish that multiple voltage-gated ion channels can alter plasticity rules at a given synapse, not by directly affecting synaptic currents, but through their ability to modulate local dendritic excitability. These results underline the heavy mutual interdependence of synaptic and intrinsic properties/plasticity in regulating homeostasis and learning in single neurons and their networks under both physiological and pathological brain states.

ACKNOWLEDGMENTS

Present address for R. Narayanan: Molecular Biophysics Unit, Indian Institute of Science, Bangalore 560012, India.

GRANTS

This work was supported by The International Human Frontier Science Program Organization to. R Narayanan and National Institutes of Health Grants MH-48432, MH-44754, and NS-37444 to D. Johnston.

DISCLOSURES

No conflicts of interest, financial or otherwise, are declared by the authors.

REFERENCES

Abbott LF, Nelson SB. Synaptic plasticity: taming the beast. *Nat Neurosci* 3: 1178–1183, 2000.

Abraham WC. Metaplasticity: tuning synapses and networks for plasticity. *Nat Rev Neurosci* 9: 387, 2008.

Abraham WC, Bear MF. Metaplasticity: the plasticity of synaptic plasticity. *Trends Neurosci* 19: 126–130, 1996.

Abraham WC, Mason-Parker SE, Bear MF, Webb S, Tate WP. Heterosynaptic metaplasticity in the hippocampus in vivo: a BCM-like modifiable threshold for LTP. *Proc Natl Acad Sci USA* 98: 10924–10929, 2001.

Abraham WC, Tate WP. Metaplasticity: a new vista across the field of synaptic plasticity. *Prog Neurobiol* 52: 303–323, 1997.

Ajay SM, Bhalla US. Synaptic plasticity in vitro and in silico: insights into an intracellular signaling maze. *Physiology (Bethesda)* 21: 289–296, 2006.

Alvarez VA, Sabatini BL. Anatomical and physiological plasticity of dendritic spines. *Annu Rev Neurosci* 30: 79–97, 2007.

Andrasfalvy BK, Magee JC. Distance-dependent increase in AMPA receptor number in the dendrites of adult hippocampal CA1 pyramidal neurons. *J Neurosci* 21: 9151–9159, 2001.

Andrasfalvy BK, Magee JC. Changes in AMPA receptor currents following LTP induction on rat CA1 pyramidal neurones. *J Physiol* 559: 543–554, 2004.

Barco A, Alarcon JM, Kandel ER. Expression of constitutively active CREB protein facilitates the late phase of long-term potentiation by enhancing synaptic capture. *Cell* 108: 689–703, 2002.

Barrionuevo G, Schottler F, Lynch G. The effects of repetitive low frequency stimulation on control and "potentiated" synaptic responses in the hippocampus. *Life Sci* 27: 2385–2391, 1980.

Bear MF. Mechanism for a sliding synaptic modification threshold. *Neuron* 15: 1–4, 1995.

Bear MF. Bidirectional synaptic plasticity: from theory to reality. *Philos Trans R Soc Lond B Biol Sci* 358: 649–655, 2003.

Bear MF, Cooper LN, Ebner FF. A physiological basis for a theory of synapse modification. *Science* 237: 42–48, 1987.

Beck H, Yaari Y. Plasticity of intrinsic neuronal properties in CNS disorders. *Nat Rev Neurosci* 9: 357–369, 2008.

Bernard C, Shah M, Johnston D. Dendrites and disease. In: *Dendrites*, edited by Stuart G, Spruston N, Hausser M. Oxford, UK: Oxford University Press, 2007, p. 531–550.

Biel M, Wahl-Schott C, Michalakis S, Zong X. Hyperpolarization-activated cation channels: from genes to function. *Physiol Rev* 89: 847–885, 2009.

Bienenstock EL, Cooper LN, Munro PW. Theory for the development of neuron selectivity: orientation specificity and binocular interaction in visual cortex. *J Neurosci* 2: 32–48, 1982.

Bliss TV, Collingridge GL. A synaptic model of memory: long-term potentiation in the hippocampus. *Nature* 361: 31–39, 1993.

Bliss TV, Lomo T. Long-lasting potentiation of synaptic transmission in the dentate area of the anaesthetized rabbit following stimulation of the perforant path. *J Physiol* 232: 331–356, 1973.

Brager DH, Johnston D. Plasticity of intrinsic excitability during long-term depression is mediated through mGluR-dependent changes in $I_{(h)}$ in hippocampal CA1 pyramidal neurons. *J Neurosci* 27: 13926–13937, 2007.

Campanac E, Daoudal G, Ankri N, Debanne D. Downregulation of dendritic $I_{(h)}$ in CA1 pyramidal neurons after LTP. *J Neurosci* 28: 8635–8643, 2008.

Canavier CC. Sodium dynamics underlying burst firing and putative mechanisms for the regulation of the firing pattern in midbrain dopamine neurons: a computational approach. *J Comput Neurosci* 6: 49–69, 1999.

Carnevale NT, Hines ML. *The NEURON Book*. Cambridge, MA: Cambridge University Press, 2006.

Chen X, Johnston D. Constitutively active G-protein-gated inwardly rectifying K^+ channels in dendrites of hippocampal CA1 pyramidal neurons. *J Neurosci* 25: 3787–3792, 2005.

Chung HJ, Ge WP, Qian X, Wiser O, Jan YN, Jan LY. G protein-activated inwardly rectifying potassium channels mediate depotentiation of long-term potentiation. *Proc Natl Acad Sci USA* 106: 635–640, 2009.

Cooper LN, Intrator N, Blais BS, Shouval HZ. *Theory of Cortical Plasticity*. Singapore: World Scientific Publishing Company, 2004.

Crepel V, Epsztein J, Ben-Ari Y. Ischemia induces short- and long-term remodeling of synaptic activity in the hippocampus. *J Cell Mol Med* 7: 401–407, 2003.

Derkach VA, Oh MC, Guire ES, Soderling TR. Regulatory mechanisms of AMPA receptors in synaptic plasticity. *Nat Rev Neurosci* 8: 101–113, 2007.

Dingledine R, Borges K, Bowie D, Traynelis SF. The glutamate receptor ion channels. *Pharmacol Rev* 51: 7–61, 1999.

Dudek SM, Bear MF. Homosynaptic long-term depression in area CA1 of hippocampus and effects of N-methyl-D-aspartate receptor blockade. *Proc Natl Acad Sci USA* 89: 4363–4367, 1992.

Errington ML, Bliss TV, Richter-Levin G, Yenk K, Doyere V, Laroche S. Stimulation at 1–5 Hz does not produce long-term depression or depotentiation in the hippocampus of the adult rat in vivo. *J Neurophysiol* 74: 1793–1799, 1995.

Fan Y, Fricker D, Brager DH, Chen X, Lu HC, Chitwood RA, Johnston D. Activity-dependent decrease of excitability in rat hippocampal neurons through increases in $I_{(h)}$. *Nat Neurosci* 8: 1542–1551, 2005.

Flavell SW, Greenberg ME. Signaling mechanisms linking neuronal activity to gene expression and plasticity of the nervous system. *Annu Rev Neurosci* 31: 563–590, 2008.

Frick A, Magee J, Johnston D. LTP is accompanied by an enhanced local excitability of pyramidal neuron dendrites. *Nat Neurosci* 7: 126–135, 2004.

Froemke RC, Poo MM, Dan Y. Spike-timing-dependent synaptic plasticity depends on dendritic location. *Nature* 434: 221–225, 2005.

Fujii S, Saito K, Miyakawa H, Ito K, Kato H. Reversal of long-term potentiation (depotentiation) induced by tetanus stimulation of the input to CA1 neurons of guinea pig hippocampal slices. *Brain Res* 555: 112–122, 1991.

Gasparini S, Migliore M, Magee JC. On the initiation and propagation of dendritic spikes in CA1 pyramidal neurons. *J Neurosci* 24: 11046–11056, 2004.

Gold JI, Bear MF. A model of dendritic spine Ca^{2+} concentration exploring possible bases for a sliding synaptic modification threshold. *Proc Natl Acad Sci USA* 91: 3941–3945, 1994.

Hausser M, Major G, Stuart GJ. Differential shunting of EPSPs by action potentials. *Science* 291: 138–141, 2001.

Hoffman DA, Magee JC, Colbert CM, Johnston D. K^+ channel regulation of signal propagation in dendrites of hippocampal pyramidal neurons. *Nature* 387: 869–875, 1997.

Holland LL, Wagner JJ. Primed facilitation of homosynaptic long-term depression and depotentiation in rat hippocampus. *J Neurosci* 18: 887–894, 1998.

Hu H, Vervaeke K, Graham LJ, Storm JF. Complementary theta resonance filtering by two spatially segregated mechanisms in CA1 hippocampal pyramidal neurons. *J Neurosci* 29: 14472–14483, 2009.

Hu H, Vervaeke K, Storm JF. Two forms of electrical resonance at theta frequencies, generated by M-current, h-current and persistent Na^+ current in rat hippocampal pyramidal cells. *J Physiol* 545: 783–805, 2002.

Hu H, Vervaeke K, Storm JF. M-channels (Kv7/KCNQ channels) that regulate synaptic integration, excitability, and spike pattern of CA1 pyramidal cells are located in the perisomatic region. *J Neurosci* 27: 1853–1867, 2007.

Huang YY, Malenka RC. Examination of TEA-induced synaptic enhancement in area CA1 of the hippocampus: the role of voltage-dependent Ca^{2+} channels in the induction of LTP. *J Neurosci* 13: 568–576, 1993.

Hutcheon B, Yarom Y. Resonance, oscillation and the intrinsic frequency preferences of neurons. *Trends Neurosci* 23: 216–222, 2000.

Jahr CE, Stevens CF. Voltage dependence of NMDA-activated macroscopic conductances predicted by single-channel kinetics. *J Neurosci* 10: 3178–3182, 1990.

Johnston D, Christie BR, Frick A, Gray R, Hoffman DA, Schexnayder LK, Watanabe S, Yuan LL. Active dendrites, potassium channels and synaptic plasticity. *Philos Trans R Soc Lond B Biol Sci* 358: 667–674, 2003.

Johnston D, Narayanan R. Active dendrites: colorful wings of the mysterious butterflies. *Trends Neurosci* 31: 309–316, 2008.

Johnston D, Williams S, Jaffe D, Gray R. NMDA-receptor-independent long-term potentiation. *Annu Rev Physiol* 54: 489–505, 1992.

Jorntell H, Hansel C. Synaptic memories upside down: bidirectional plasticity at cerebellar parallel fiber-Purkinje cell synapses. *Neuron* 52: 227–238, 2006.

Kalantzis G, Shouval HZ. Structural plasticity can produce metaplasticity. *PLoS One* 4: e8062, 2009.

Kemp N, McQueen J, Faulkes S, Bashir ZI. Different forms of LTD in the CA1 region of the hippocampus: role of age and stimulus protocol. *Eur J Neurosci* 12: 360–366, 2000.

Kennedy MB, Beale HC, Carlisle HJ, Washburn LR. Integration of biochemical signalling in spines. *Nat Rev Neurosci* 6: 423–434, 2005.

Kerchner GA, Nicoll RA. Silent synapses and the emergence of a postsynaptic mechanism for LTP. *Nat Rev Neurosci* 9: 813–825, 2008.

Kim J, Jung SC, Clemens AM, Petralia RS, Hoffman DA. Regulation of dendritic excitability by activity-dependent trafficking of the A-type K^+ channel subunit Kv4.2 in hippocampal neurons. *Neuron* 54: 933–947, 2007.

Kirkwood A, Rioult MC, Bear MF. Experience-dependent modification of synaptic plasticity in visual cortex. *Nature* 381: 526–528, 1996.

Leite JP, Neder L, Arisi GM, Carlotti CG Jr, Assirati JA, Moreira JE. Plasticity, synaptic strength, and epilepsy: what can we learn from ultrastructural data? *Epilepsia* 46 Suppl. 5: 134–141, 2005.

Lisman J. A mechanism for the Hebb and the anti-Hebb processes underlying learning and memory. *Proc Natl Acad Sci USA* 86: 9574–9578, 1989.

Lisman J, Raghavachari S. A unified model of the presynaptic and postsynaptic changes during LTP at CA1 synapses. *Sci STKE 2006*: re11, 2006.

Lisman JE. Three Ca^{2+} levels affect plasticity differently: the LTP zone, the LTD zone and no man's land. *J Physiol* 532: 285, 2001.

Lisman JE. The pre/post LTP debate. *Neuron* 63: 281–284, 2009.

Liu L, Wong TP, Pozza MF, Lingenhoehl K, Wang Y, Sheng M, Auberson YP, Wang YT. Role of NMDA receptor subtypes in governing the direction of hippocampal synaptic plasticity. *Science* 304: 1021–1024, 2004.

Lorincz A, Notomi T, Tamas G, Shigemoto R, Nusser Z. Polarized and compartment-dependent distribution of HCN1 in pyramidal cell dendrites. *Nat Neurosci* 5: 1185–1193, 2002.

Losonczy A, Makara JK, Magee JC. Compartmentalized dendritic plasticity and input feature storage in neurons. *Nature* 452: 436–441, 2008.

Lujan R, Maylie J, Adelman JP. New sites of action for GIRK and SK channels. *Nat Rev Neurosci* 10: 475–480, 2009.

Magee JC. Dendritic hyperpolarization-activated currents modify the integrative properties of hippocampal CA1 pyramidal neurons. *J Neurosci* 18: 7613–7624, 1998.

Magee JC. Dendritic Ih normalizes temporal summation in hippocampal CA1 neurons. *Nat Neurosci* 2: 848, 1999.

Malenka RC, Bear MF. LTP and LTD: an embarrassment of riches. *Neuron* 44: 5–21, 2004.

Massey PV, Bashir ZI. Long-term depression: multiple forms and implications for brain function. *Trends Neurosci* 30: 176–184, 2007.

Mayer ML, Westbrook GL. Permeation and block of N-methyl-D-aspartic acid receptor channels by divalent cations in mouse cultured central neurones. *J Physiol* 394: 501–527, 1987.

Mayford M, Wang J, Kandel ER, O'Dell TJ. CaMKII regulates the frequency-response function of hippocampal synapses for the production of both LTD and LTP. *Cell* 81: 891–904, 1995.

McNaughton BL, Douglas RM, Goddard GV. Synaptic enhancement in fascia dentata: cooperativity among coactive afferents. *Brain Res* 157: 277–293, 1978.

Migliore M, Hoffman DA, Magee JC, Johnston D. Role of an A-type K^+ conductance in the back-propagation of action potentials in the dendrites of hippocampal pyramidal neurons. *J Comput Neurosci* 7: 5–15, 1999.

Migliore M, Shepherd G. Emerging rules for the distributions of active dendritic conductances. *Nat Rev Neurosci* 3: 362–370, 2002.

Moody WJ, Bosma MM. Ion channel development, spontaneous activity, and activity-dependent development in nerve and muscle cells. *Physiol Rev* 85: 883–941, 2005.

Narayanan R, Johnston D. Long-term potentiation in rat hippocampal neurons is accompanied by spatially widespread changes in intrinsic oscillatory dynamics and excitability. *Neuron* 56: 1061–1075, 2007.

Narayanan R, Johnston D. The h channel mediates location dependence and plasticity of intrinsic phase response in rat hippocampal neurons. *J Neurosci* 28: 5846–5860, 2008.

Newpher TM, Ehlers MD. Glutamate receptor dynamics in dendritic microdomains. *Neuron* 58: 472–497, 2008.

Pape H. Queer current and pacemaker: the hyperpolarization-activated cation current in neurons. *Annu Rev Physiol* 58: 299–327, 1996.

Philpot BD, Espinosa JS, Bear MF. Evidence for altered NMDA receptor function as a basis for metaplasticity in visual cortex. *J Neurosci* 23: 5583–5588, 2003.

Philpot BD, Sekhar AK, Shouval HZ, Bear MF. Visual experience and deprivation bidirectionally modify the composition and function of NMDA receptors in visual cortex. *Neuron* 29: 157–169, 2001.

Poirazi P, Brannon T, Mel BW. Arithmetic of subthreshold synaptic summation in a model CA1 pyramidal cell. *Neuron* 37: 977–987, 2003.

Polsky A, Mel BW, Schiller J. Computational subunits in thin dendrites of pyramidal cells. *Nat Neurosci* 7: 621–627, 2004.

Poolos NP, Migliore M, Johnston D. Pharmacological upregulation of h-channels reduces the excitability of pyramidal neuron dendrites. *Nat Neurosci* 5: 767–774, 2002.

Reid IC, Stewart CA. Seizures, memory and synaptic plasticity. *Seizure* 6: 351–359, 1997.

Robinson RB, Siegelbaum SA. Hyperpolarization-activated cation currents: from molecules to physiological function. *Annu Rev Physiol* 65: 453–480, 2003.

Rosenkranz JA, Frick A, Johnston D. Kinase-dependent modification of dendritic excitability after long-term potentiation. *J Physiol* 587: 115–125, 2009.

Sacktor TC. PKMzeta, LTP maintenance, and the dynamic molecular biology of memory storage. *Prog Brain Res* 169: 27–40, 2008.

Sajikumar S, Navakkode S, Frey JU. Protein synthesis-dependent long-term functional plasticity: methods and techniques. *Curr Opin Neurobiol* 15: 607–613, 2005.

Saudargiene A, Porr B, Worgotter F. Local learning rules: predicted influence of dendritic location on synaptic modification in spike-timing-dependent plasticity. *Biol Cybern* 92: 128–138, 2005.

Scharfman HE. The neurobiology of epilepsy. *Curr Neurol Neurosci Rep* 7: 348–354, 2007.

Schulz PE, Cook EP, Johnston D. Changes in paired-pulse facilitation suggest presynaptic involvement in long-term potentiation. *J Neurosci* 14: 5325–5337, 1994.

Shah NT, Yeung LC, Cooper LN, Cai Y, Shouval HZ. A biophysical basis for the inter-spike interaction of spike-timing-dependent plasticity. *Biol Cybern* 95: 113–121, 2006.

Shepherd JD, Huganir RL. The cell biology of synaptic plasticity: AMPA receptor trafficking. *Annu Rev Cell Dev Biol* 23: 613–643, 2007.

Shouval HZ, Bear MF, Cooper LN. A unified model of NMDA receptor-dependent bidirectional synaptic plasticity. *Proc Natl Acad Sci USA* 99: 10831–10836, 2002.

Sjostrom PJ, Hausser M. A cooperative switch determines the sign of synaptic plasticity in distal dendrites of neocortical pyramidal neurons. *Neuron* 51: 227–238, 2006.

Sjostrom PJ, Rancz EA, Roth A, Hausser M. Dendritic excitability and synaptic plasticity. *Physiol Rev* 88: 769–840, 2008.

Smith MA, Ellis-Davies GC, Magee JC. Mechanism of the distance-dependent scaling of Schaffer collateral synapses in rat CA1 pyramidal neurons. *J Physiol* 548: 245–258, 2003.

Song S, Miller KD, Abbott LF. Competitive Hebbian learning through spike-timing-dependent synaptic plasticity. *Nat Neurosci* 3: 919–926, 2000.

Turrigiano GG. Homeostatic plasticity in neuronal networks: the more things change, the more they stay the same. *Trends Neurosci* 22: 221–227, 1999.

Turrigiano GG, Nelson SB. Hebb and homeostasis in neuronal plasticity. *Curr Opin Neurobiol* 10: 358–364, 2000.

Turrigiano GG, Nelson SB. Homeostatic plasticity in the developing nervous system. *Nat Rev Neurosci* 5: 97–107, 2004.

Ulrich D. Dendritic resonance in rat neocortical pyramidal cells. *J Neurophysiol* 87: 2753–2759, 2002.

Wang H, Wagner JJ. Priming-induced shift in synaptic plasticity in the rat hippocampus. *J Neurophysiol* 82: 2024–2028, 1999.

Wang Z, Xu NL, Wu CP, Duan S, Poo MM. Bidirectional changes in spatial dendritic integration accompanying long-term synaptic modifications. *Neuron* 37: 463–472, 2003.

Watt AJ, Sjostrom PJ, Hausser M, Nelson SB, Turrigiano GG. A proportional but slower NMDA potentiation follows AMPA potentiation in LTP. *Nat Neurosci* 7: 518–524, 2004.

Williams SR. Spatial compartmentalization and functional impact of conductance in pyramidal neurons. *Nat Neurosci* 7: 961–967, 2004.

Willshaw DJ, Dayan P. Optimal plasticity in matrix memories: what goes up must come down. *Neural Comput* 2: 85–93, 1990.

Yeung LC, Shouval HZ, Blais BS, Cooper LN. Synaptic homeostasis and input selectivity follow from a calcium-dependent plasticity model. *Proc Natl Acad Sci USA* 101: 14943–14948, 2004.

Yu X, Shouval HZ, Knierim JJ. A biophysical model of synaptic plasticity and metaplasticity can account for the dynamics of the backward shift of hippocampal place fields. *J Neurophysiol* 100: 983–992, 2008.

Zhang W, Linden DJ. The other side of the engram: experience-driven changes in neuronal intrinsic excitability. *Nat Rev Neurosci* 4: 885–900, 2003.

Zucker RS. Calcium- and activity-dependent synaptic plasticity. *Curr Opin Neurobiol* 9: 305–313, 1999.